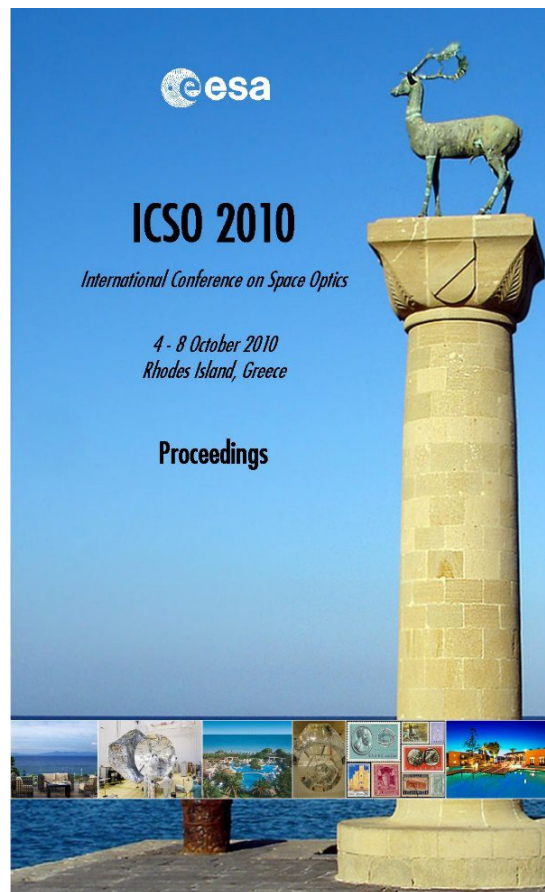


# International Conference on Space Optics—ICSO 2010

Rhodes Island, Greece

4–8 October 2010

*Edited by Errico Armandillo, Bruno Cugny,  
and Nikos Karafolas*



## *The integral field unit for the James Webb space telescope's near-infrared spectrograph*

*David J. Purl, Daniel R. Lobb, Andrew R. Barnes,  
R. Gordon Talbot, et al.*



International Conference on Space Optics — ICSO 2010, edited by Errico Armandillo, Bruno Cugny,  
Nikos Karafolas, Proc. of SPIE Vol. 10565, 105650J · © 2010 ESA and CNES  
CCC code: 0277-786X/17/\$18 · doi: 10.1117/12.2309221

## THE INTEGRAL FIELD UNIT FOR THE JAMES WEBB SPACE TELESCOPE'S NEAR-INFRARED SPECTROGRAPH

David J Purll<sup>1</sup>, Daniel R Lobb<sup>1</sup>, Andrew R Barnes<sup>1</sup>, R Gordon Talbot<sup>2</sup>, Stephen Rolt<sup>2</sup>, David J Robertson<sup>2</sup>,  
Martin F Closs<sup>3</sup>, Maurice te Plate<sup>4</sup>

<sup>1</sup>Surrey Satellite Technology Ltd., Rayleigh House, 1 Bat & Ball Road, Sevenoaks, TN14 5LJ, UK

<sup>2</sup>CfAI, Durham University, Netpark Research Institute, Joseph Swan Road, Sedgefield, TS21 3FB, UK

<sup>3</sup>EADS Astrium GmbH, p.o. box 80 11 69, D-81663 Munich, Germany

<sup>4</sup>European Space Agency, Keplerlaan 1, PO Box 299, 2200 AG, Noordwijk, The Netherlands

### I. INTRODUCTION

The European Space Agency (ESA) is providing the Near Infrared Spectrograph (NIRSpec) developed by EADS Astrium GmbH to fly on the James Webb Space Telescope (JWST). NIRSpec covers the 0.6-5.0  $\mu\text{m}$  domain. It will be primarily operated as a multi-object spectrograph, using a MEMS micro-shutter array (MSA) provided by NASA to select multiple objects from the field of view at an intermediate image plane formed by the NIRSpec fore-optics. The MSA apertures form multiple entrance slits of the spectrometer section.

In addition, an integral field unit (IFU) will receive light through an aperture in the MSA support structure, sampling a 3 x 3 arcsec sub-field of view in the same image plane (see Fig. 1). The IFU will enable a 2-D spectral map to be acquired of an extended object such as a galaxy. In order to acquire the 2-D array of spectra without overlaps, the square sub-field must be sliced up by the IFU into 30 slices and re-arranged into a single line of virtual slits to enter the spectrometer section. Further details of this application have been given previously [1].

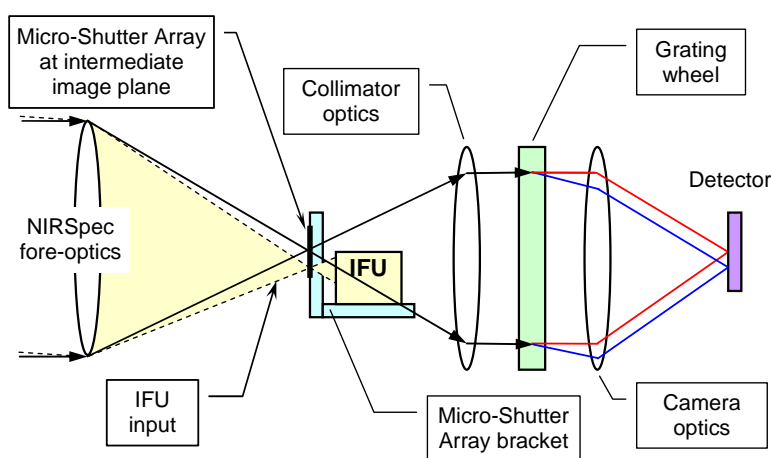


Fig. 1. Schematic of the NIRSpec instrument as relevant to the IFU

The IFU uses a very innovative optical design, developed by Surrey Satellite Technology Ltd (SSTL) in consultation with its subcontractor, the Centre for Advanced Instrumentation (CfAI) of Durham University, which had developed earlier types of image-slicing IFUs using monolithic diamond-machined mirrors [2], [3]. The design adopted makes full use of state-of-the-art diamond machining techniques available at CfAI for producing the mirrors. The manufacture, assembly and optical testing of the IFU were performed by SSTL and the cryogenic cycling of the unit with associated further optical testing was performed by CfAI.

### II. REQUIREMENTS AND OPTICAL DESIGN OF THE IFU

The required input and output geometry, as seen from the spectrometer, is shown in Fig. 2. The input field, formed at  $f/12.5$  by the telescope and NIRSpec fore-optics, is 1.2mm x 1.2mm. The IFU splits this field into 30 slices, each 1.2mm x 0.04mm at the input field. It images these slices in a common line, forming a “virtual slit” with 30 sub-slits, which is formed in the same plane as the input field. All sub-slit images are telecentric with the input, so that the IFU output is correctly collimated, dispersed and re-imaged by the spectrometer optics.

The magnification of the IFU is unity in the direction parallel with the virtual slit, but x2 in the orthogonal direction which is the dispersion direction in the spectrometer system. Each sub-slit is 1.2mm long and 0.08mm wide. The sub-slits are arranged in two groups of 15 with a gap in the middle to allow for the obscuration of the pick-off mirror. The overall length of the virtual slit is around 75mm.

The IFU was a relatively late addition to NIRSpec and must fit in the MSA support structure in a very limited envelope, standing back significantly from the image plane. Because of these constraints, the powers of the optical surfaces and the extreme angles of incidence tend to be large. This generates design aberrations that must be reduced by using relatively complex mirror shapes to achieve the required performance, shapes almost impossible to make without the free-form possibilities offered by 5-axis diamond machining.

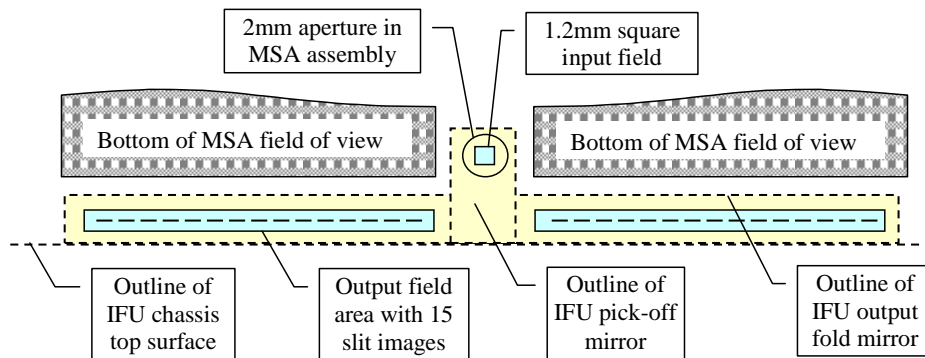


**Fig. 2.** Schematic of the input and output geometry for the IFU fields of view (not to scale)

The IFU must survive temperature cycling between integration and test at normal terrestrial temperatures and operation at around 30K, and should provide good optical performance at both extremes. This could only be achieved with an extremely athermal assembly. This led to the adoption of an aluminium chassis structure to match the diamond-machined aluminium mirrors, all cut from the same billet of 6061 aluminium.

The principal performance requirements for the IFU are the properties shown in Table 1. The wavefront error (WFE) specification includes defocus caused by inaccuracies in initial location of the IFU and shifts due to cool-down. There are many other performance requirements, mainly in respect of detailed geometrical properties and mechanical alignment stability, which are not reported in detail in this paper due to lack of space.

**Table 1.** Main performance requirements of the IFU

Performance wavelength range	0.7 – 5.0 $\mu\text{m}$ (functional range 0.6 – 5.0 $\mu\text{m}$ )
Throughput	> 50%
Wavefront error	< 97 nm rms
Telecentricity errors	< 0.2°
Stray light	< 5% sub-slit cross-talk

Fig. 3 gives an overall impression of the optical layout and for clarity shows only 4 slices, corresponding to the two inner and two outer sub-slits in each half of the virtual output slit (4 out of 30 facets on the slicer, pupil mirror and slit mirror arrays are shown). The optical design has been reported in more detail previously [4], [5].

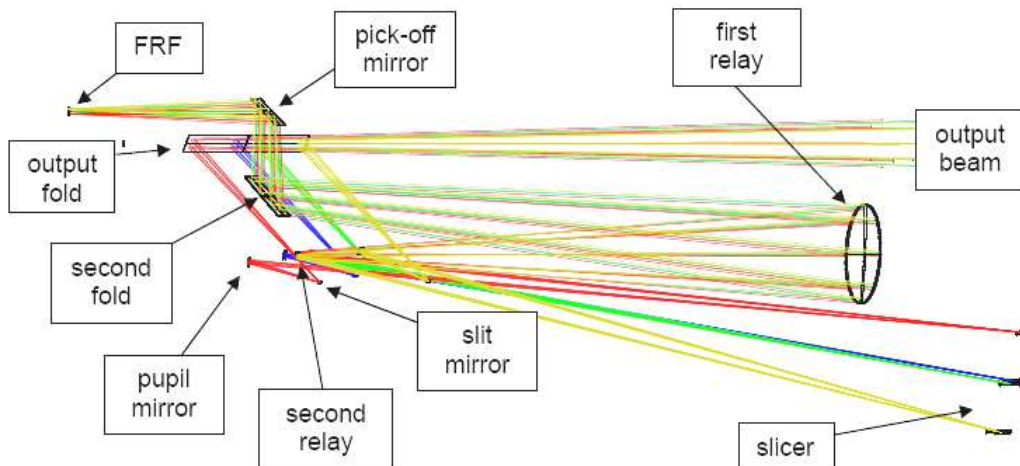


**Fig. 3.** Optical layout of the IFU (only 4 of 30 slices shown). FRF indicates the input field reference frame.

Two flat mirrors, a pick-off and a second fold, direct the beam from the input field into the IFU. Problems in achieving the optical performance are increased because the pick-off mirror cannot be placed at the image plane. Two re-imaging (relay) mirrors form a magnified intermediate image of the input field on the slicer. A telephoto arrangement is used, with a concave relay 1 and a convex relay 2. Anamorphic magnification,  $\times 10$  in

the spatial and x20 in the spectral sections, is introduced by the relay mirrors, which are toroids with cubic perturbations. The three array components are shown in Fig. 4. The slicer splits the magnified intermediate image at 30 mirror facets which direct the beamlets on to the pupil mirror array. Each slicer facet, 0.8mm by 12mm, is curved and tilted uniquely on two axes and is made slightly toric, to correct for astigmatism in pupil imaging by the relay mirrors. The pupil mirrors are curved and tilted to form sub-slit images in a common line – effectively the entrance slit of the spectrometer – close to the surfaces of the “slit” mirrors. The relay 2 mirror is located between the two groups of pupil mirrors, and is machined on the same substrate although it is a totally different entity, a significant advantage enabled by the free-form diamond machining. The pupil mirrors are concave toroids with added cubic perturbations, tilted on two axes. The slit mirrors, concave and spherical, are tilted in such a way that all output beams are directed towards a common spectrometer entrance pupil. The NIRSpec IFU differs from some previous systems in that the slit mirrors cannot be located at a focal plane. They are followed by an output fold mirror (fold 3), which reflects the output beam towards the spectrometer.

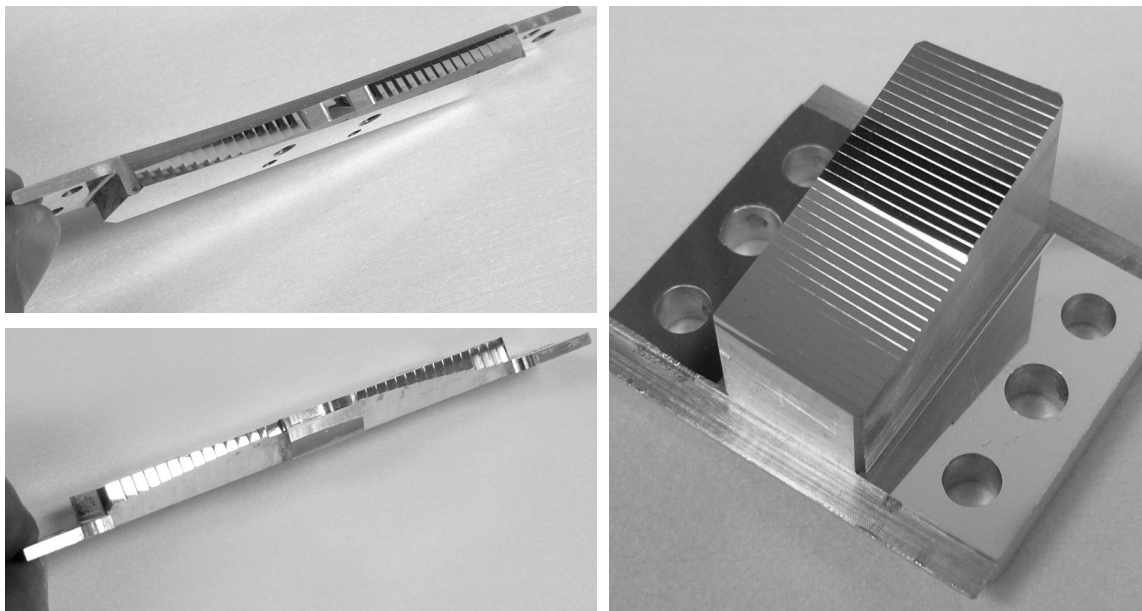


**Fig. 4.** The mirror arrays (clockwise, from right: slicer; slits; pupils with relay 2 at the centre)  
The slicer has an active area around 25 x 12.5mm, and the long arrays an active length around 75mm.

### III. MANUFACTURING METHODS

An all-aluminium design was adopted, using diamond machining to produce not only the optical surfaces but also the critical mounting interfaces for the mirrors. The same billet of 6061 aluminium alloy was used for both mirrors and chassis. Each of the 3 arrays was machined as a monolithic component in a single complex machining operation, without remounting. This approach yields a perfectly athermal design, very precise relative control of the mirror facets within the arrays, and simplification of the build (91 out of a total of 95 mirror surfaces are pre-aligned on only 3 components). The mirrors are coated with a protected gold coating.

The slicer, pupil mirrors (with relay 2) and slit mirrors were formed by raster fly-cutting. In this process, the cutting tool is rotated while the work-piece is moved on 3 axes, so that the required surface shape is generated in a series of “pecks”. Half-radius tool points and rotation of the work-piece on the 5<sup>th</sup> axis were used to minimize the dead space between mirrors. Relay 1 was produced by slow-slide-servo turning, a turning operation modified by controlled movements of the tool during each work-piece rotation, to perturb the surface shape from axial symmetry. The flat fold mirrors were produced by conventional fly-cutting.

Scattering losses attributed to the surface roughness of the mirrors are a key part of the throughput budget at short wavelengths. The achieved roughness values are given in Table 2. The higher values correspond with the most complex mirrors, which have to be raster fly-cut. New research shows that roughness values could be improved considerably in future using rapid-solidified aluminium alloy. Values as low as 2-3 nm can be expected for some components and it may be possible to achieve roughness of less than 5 nm on a routine basis.

**Table 2.** Achieved roughness values of the FM mirrors (nm rms).

Fold 1	4.69 - 7.5	Fold 3	2.69 - 7.16	Relay 2	13.69 - 18.11	Pupils	5.32 - 8.39
Fold 2	5.58 - 8.41	Relay 1	4.11 - 8.64	Slicer	11.9 - 20.6	Slits	4.3 - 13.2

#### IV. IFU ASSEMBLY AND ALIGNMENT

The IFU assembly is shown mounted on its transport plate in Fig. 5. The mass is 825g and the dimensions are 140mm wide (excluding the mounting feet) x 213mm long (including slicer screw heads) and x 71mm high (excluding the pick-off mirror). The design requires only three components to be adjusted, namely the relay 1 mirror and the slicer and slit mirror arrays. The mirror adjustment method involves sliding the mirror flanges over flat mounting interfaces, using oversized mounting screw holes, and shimming where necessary to adjust positions orthogonal to the mounting planes. All elements were pinned and glued after adjustments. Mounting surfaces for the mirrors were diamond-machined to be as flat as possible and the mounting flanges designed such that strain introduced by residual imperfections in these mating surfaces is not transferred (as far as possible) to mirror surfaces. Nevertheless, mounting strain does produce significant astigmatism at the first relay mirror, and this is the principal cause of reduction in optical performance. (An IFU with a WFE of around 50nm rms could have been produced if further iterations of the relay 1 mounting flange design or of the interface machining techniques had been possible within the project constraints.)

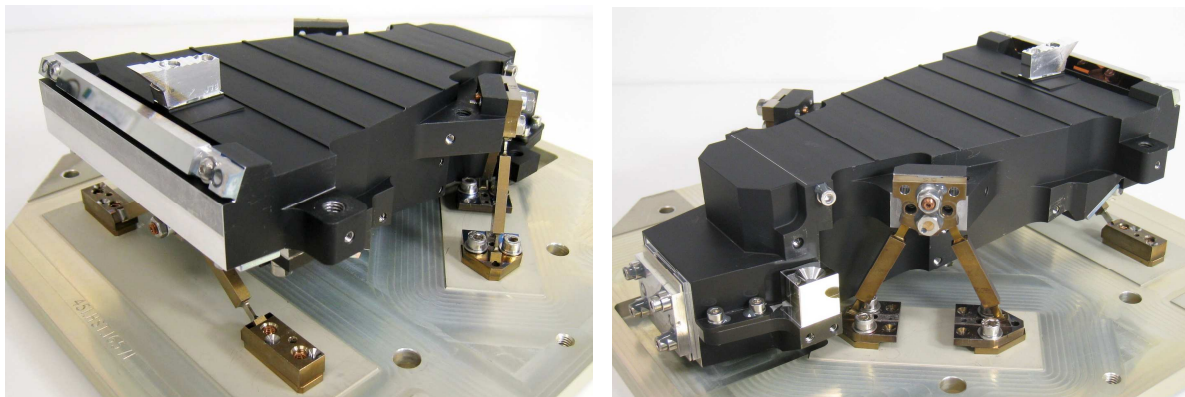


**Fig. 5.** The flight model IFU assembly (left: front view, right: rear view)

The other main issue in the mechanical design is to avoid distortion of the chassis over the very large, approximately 250K difference between assembly and operating temperatures, which would to some extent pass through to the mirrors and hence result in reduced optical quality. The aluminium IFU is mounted on a titanium assembly, the MSA bracket, so the differential expansion is considerable. To avoid stress on cool-down, the IFU is therefore mounted on flexible bipod legs forming an isostatic mount, clearly seen in the photographs. However, positionally, such a mount maintains the isostatic centre, not the optical geometry, and so the relative position with respect to the input reference frame will change, both vertically and along the optical axis. These positional offsets have to be taken into account when integrating the IFU with NIRSpec at room temperature.

In spite of the considerable flexibility of the legs, the unit and the geometrical properties of the output slits must maintain a stable position and alignment to within around 10 micrometers after vibration and thermal cycling, so the whole design is mechanically very challenging. During final testing, the position of the optical reference frame and the direction of the optical axis were measured with respect to an alignment cube and laser tracking ball. This information is used by Astrium when integrating the unit into NIRSpec. The alignment cube, incorporating a cone-shaped recess for the laser tracking ball, can be seen in the right hand photograph.

#### V. CRYOGENIC TESTING

In the JWST the unit is expected to operate between 30K and 44K. Cryogenic testing was performed in a dedicated vacuum chamber at CfAI with the IFU mounted on a titanium test plate to simulate the interface to the MSA assembly in NIRSpec. The IFU was first baked out at 325K (encompassing the survival requirement, 315K) and was then cycled between 305K and a minimum defined by the chamber capability. Optical testing was performed at around 36K and at room temperature. A total of 8 cycles was performed for the Qualification Model and 4 for the Flight Model. For one cycle, a lower temperature below 22K was reached as a cold survival test, by blocking the optical windows to prevent thermal radiation entering the chamber.

The principal optical test set-up used during cryogenic testing is shown in Fig. 6. A Shack-Hartmann wavefront sensor was used to measure the WFE. A similar set-up was used for geometrical measurements with the reference sphere replaced by a duo-lateral detector, thus performing a knife-edge test on the slicer image at the input field position. Movement of the input field position relative to the IFU hardware during cool-down was shown to be quite close to the predictions from finite element analysis of the design (0.285mm along the optical axis and 0.122mm vertically). More extensive testing, including input and output slit geometry, telecentricity, throughput and stray light was performed at room temperature in SSTL, before and after cryo-

cycling. The WFE test set-up used for ambient temperature tests at SSTL was similar to that shown in Fig. 6. For other tests, different input sources generating point and flat-field inputs were deployed on the XYZ scanning tables on the input side, in place of the wavefront sensor, and a radiometer head or CCD camera (configured for either pupil imaging or slit imaging) were deployed on the scanning tables on the output side.

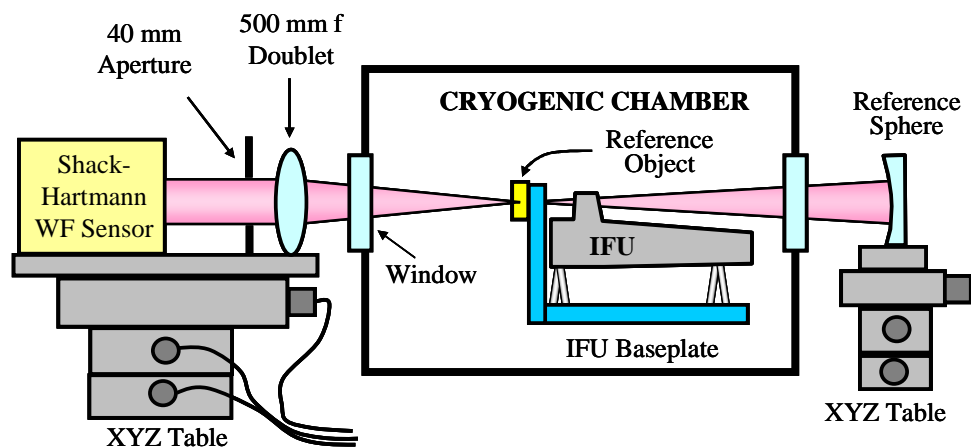


Fig. 6. The principal optical test set-up used in cryogenic tests

## VI. FLIGHT MODEL TEST RESULTS

A summary of the FM wavefront error measurements is shown in Fig. 7. The WFE appears to have improved through the test phases, and this may be due to relaxation of stresses through the vibration and cryo-cycling, although insufficient research to verify this was possible within the project. The cold test results were about 10nm rms worse on average than the ambient tests at the same cryogenic facility, not a bad result given the large contraction of the aluminium over the 250K cool-down. A summary of the telecentricity measurements is shown in Fig. 8; these were all within the 12 arc minute specification.

A typical output slit image resulting from a flat-field input is shown in Fig. 9. The small slicer facets and the low aperture of the system give rise to a somewhat blurred image, but it has to be remembered that this image is deployed over only 2 x 30 pixels on the NIRSpec detector. There is also a mottled effect (again, not resolved by the NIRSpec detector) arising from the surface roughness of the mirrors, particularly the slicer, which is in focus and on which the “pecked” effect of the raster fly-cutting is most marked. The slit image will appear more blurred in the longer NIRSpec wavelengths, out to 5 $\mu$ m.

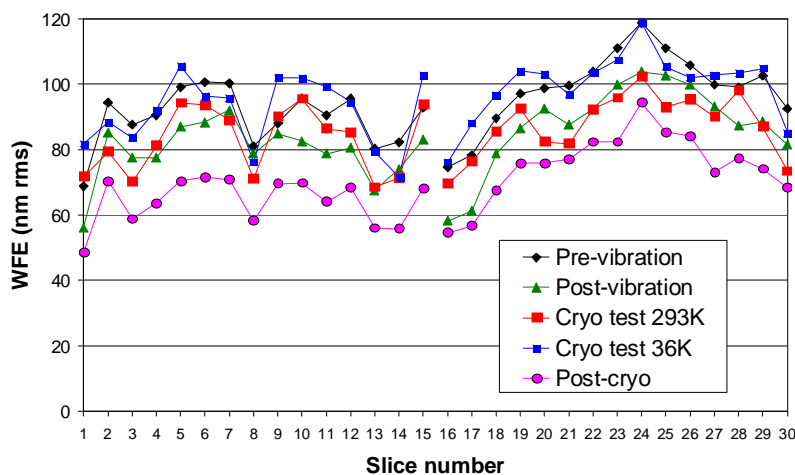


Fig. 7. WFE results summary

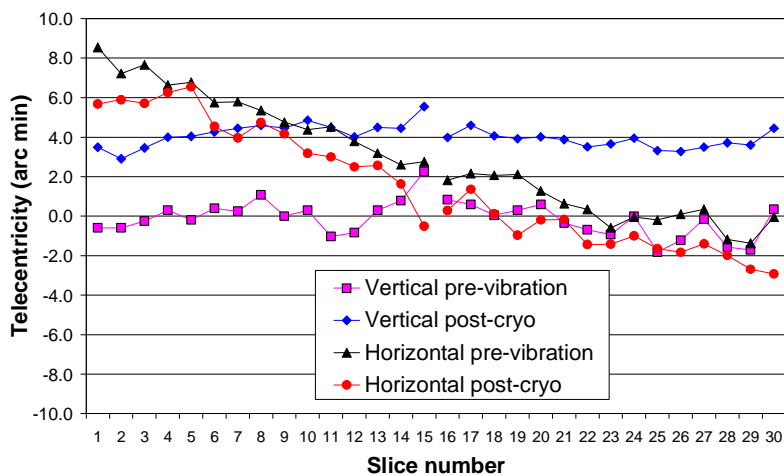


Fig. 8. Telecentricity results summary

The throughput budget, using surface scatter values calculated from the actual measured values of mirror roughness, is shown in Fig. 10. The mirrors were coated in several batches and two examples of the vendor's reflectivity measurements are included in the budgeting. It can be seen that the gold reflectivity dominates over scatter at longer wavelengths. The measured throughputs were 56 – 65% at 700nm and 79 – 86% at 905nm, which are comparable with the bands of the budget.

Stray light (cross-talk between image slices) was measured by illuminating a slit with a spot of light and measuring the percentage of that light which appears in the four slits (+/- two slits) either side of it. The cross-talk measured in this way was between 2.2 and 3.9%. Fig. 11. shows a typical result.



Fig. 9. Output image of a sub-slit (1.2mm x 0.08mm) at 905nm wavelength

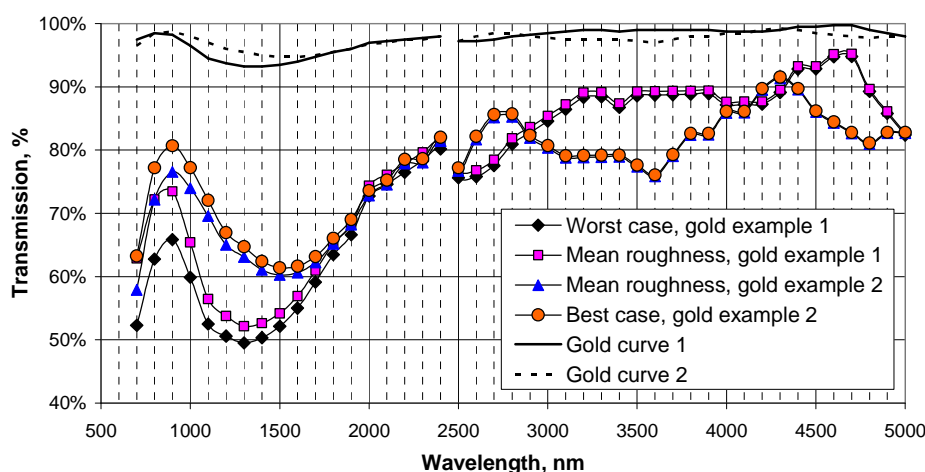


Fig. 10. Throughput budget summary

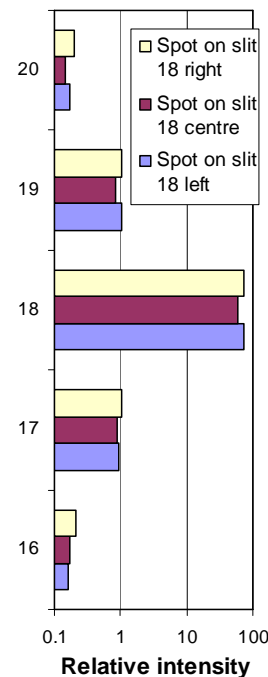


Fig. 11. Cross-talk

## VII. CONCLUSIONS

The NIRSpec IFU is at the complex end of image-slicing integral field units. The constraints have required complex optical surfaces to be used, which have benefited from, and could not have been produced without, the advantages of state-of-the-art free-form diamond machining. Environmental constraints have required the adoption of an athermal design, with aluminium mirrors mounted in an aluminium chassis. Isostatic mounting to a titanium structure has resulted in low transfer of stress to the optics in spite of the large, 250K cool-down to operating temperature, at the same time as maintaining stability in the order of 10-20µm. This extremely challenging development has met its major performance goals, albeit with some numerically-marginal waivers on some requirements. The IFU will be integrated with the flight model of NIRSpec during 2010.

## VIII. REFERENCES

- [1] M. F. Closs, P. Ferruit, D. R. Lobb, W. R. Preuss, S. Rolt and R. G. Talbot, "The Integral Field Unit on the James Webb Space Telescope's Near-Infrared Spectrograph," *Proc. SPIE*, vol. 7010, pp. 701011.1-701011.12, August 2008
- [2] R. Content, "Advanced Image Slicers for Integral Field Spectroscopy with UKIRT and Gemini," *Proc. SPIE*, vol. 3354, pp. 187-200, July 1998.
- [3] C. M. Dubbeldam, et al., "An Integral Field Unit for the Gemini Near-InfraRed Spectrograph," *Proc. SPIE*, vol. 4008, pp. 1181-1192, August 2000.
- [4] D. R. Lobb and D. J. Robertson "Design and Manufacturing Methods for the Integrated Field Unit of the NIRSpec Instrument on JWST," *Proc. 6th Intl. Conf. on Space Optics*, vol. ESA SP-621, June 2006.
- [5] D. R. Lobb, D. J. Robertson, M. F. Closs and A. R. Barnes, "Design and Manufacture of the Integral Field Unit for the NIRSpec Spectrometer on JWST," *Proc. SPIE*, vol. 7100, pp. 710012.1-710012.8, September 2008.